Subgrid parameterisations for high resolution atmospheric flows

V. Kitsios* J. S. Frederiksen* M. J. Zidikheri†

November 24, 2010

Abstract

Numerical and computational methods are developed for the Large Eddy Simulation (LES) of atmospheric flows on a sphere with a spectral quasigeostrophic model. The subgrid scales of motion are parameterised using a net eddy viscosity that is derived from a high resolution reference Direct Numerical Simulation (DNS) with 504 zonal and total wavenumbers or 1536×768 grid points (longitude $\times$ latitude). Simulations are undertaken for a wide range of truncation wavenumbers to determine the influence of resolution on the net eddy viscosity. A universal scaling law for these coefficients is established for application to LES of more general geophysical flows.

Contents

*Centre for Australian Weather and Climate Research (CAWCR), CSIRO Marine and Atmospheric Research, Aspendale 3195, Australia.

†CAWCR, Bureau of Meteorology, Melbourne, Victoria, Australia

1 Introduction

High Reynolds number atmospheric flows cover a vast range of scales making it unfeasible to adequately resolve all scales of motion. In geophysical fluid dynamics one therefore resorts to LES in which the large eddies are resolved on a computational grid and the remaining small scales are represented by a subgrid parameterisation. The first such parameterisation was the ad hoc deterministic Smagorinsky eddy viscosity model [6], in which the subgrid scale dissipation was related to the local strain rate via a specified parameter. An ad hoc stochastic version of this model was subsequently proposed by Leith [5]. Frederiksen & Davies [3] studied barotropic atmospheric flows and used turbulence closure theory to develop self consistent eddy viscosity and stochastic backscatter parameterisations with no tuning parameters needed. Frederiksen & Kepert [4] subsequently developed an essentially equivalent stochastic modelling approach, in which the eddy viscosity and stochastic backscatter terms are determined from a reference DNS data set, in an effort to widen the applicability of the closure. In this context, a DNS is understood to be a highly resolved simulation with a wavenumber dependent bare viscosity to account for the unresolved scales of motion.

The aim of the present study is to search for universal scaling laws of the wavenumber-dependent viscosity by employing the subgrid modelling method of Frederiksen & Kepert [4]. This would make the parameterisations more generally applicable and remove the need to determine them from a reference DNS. In section 2 we summarise the quasigeostrophic potential vorticity equation (QGPVE) [1, 7] used in our simulations of a turbulent baroclinic atmospheric flow. The LES version of the QGPVE is then presented in section 3, along with the details of the stochastic modelling of the subgrid scales. Various LES simulations are then undertaken in section 4 to investigate how the coefficients of the subgrid scale model change with resolution, and a universal scaling of these coefficients is proposed. In section 5 the self consistency of the scaling with the bare viscosity in the DNS is assessed, and the conclusions are presented in section 6.

2 Two-level spectral quasigeostrophic equations

For our study of subgrid scale parameterisations we employ the two-level quasigeostrophic model of Frederiksen [1]. The QGPVE is derived on the basis of hydrostatic and approximate geostrophic balance. Here, the vorticity is represented at two discrete vertical levels, with $j = 1$ representing the

upper level at 250hPa ($z \approx 10$km), and $j = 2$ the lower level at 750hPa ($z \approx 2.5$km). The system is non-dimensionalised by the radius of the Earth ($a = 6371$km) as a length scale and the inverse of the Earth's angular velocity ($\Omega = 7.292 \times 10^{-5}\text{s}^{-1}$) as a time scale.

The QGPVE is spectrally discretised by expanding the field variables in spherical harmonics with zonal (longitudinal) wavenumber m and the total wavenumber n. Note the latitudinal (meridional) wavenumber is $n-m$. The evolution equation for q^j_{mn} is given by [1]

$$\begin{aligned}\frac{\partial q^j_{mn}}{\partial t} &= \mathrm{i}\sum_{pq}\sum_{rs} K^{mpr}_{nqs}\psi^j_{-pq}q^j_{-rs} - \mathrm{i}\omega_{mn}\zeta^j_{mn} - \alpha^j\zeta^j_{mn} + \kappa_n(\tilde{q}^j_{mn} - q^j_{mn}) \\ &- \sum_{l=1}^{2} D^{jl}_0(m,n)q^j_{mn} \ , \end{aligned} \tag{1}$$

where the reduced potential vorticity spectral coefficients are

$$q^j_{mn} = \zeta^j_{mn} + (-1)^j F_L\left(\psi^1_{mn} - \psi^2_{mn}\right) \ . \tag{2}$$

Here, $\zeta^j_{mn} = -n(n+1)\psi^j_{mn}$ are the spectral coefficients of the vorticity and ψ^j_{mn} the streamfunction coefficients at level j. Also, F_L is a layer coupling parameter, which is inversely proportional to the potential temperature difference between the two levels, and related to the Rossby radius of deformation by $r_{\text{Ros}} = 1/\sqrt{2F_L}$. In (1) the summations are over the triangular truncated wavenumber set

$$\begin{aligned}\mathbf{T} = [\ p,q,r,s \mid -T \le p \le T \ , \ |p| \le q \le T \ , \\ -T \le r \le T \ , \ |r| \le s \le T \ ] \ , \end{aligned} \tag{3}$$

with T the DNS truncation wavenumber. The Rossby wave frequency $\omega_{mn} = -Bm/(n(n+1))$, where $B = 2$ with our non-dimensionalisation, and K^{mpr}_{nqs} are the interaction coefficients detailed in Frederiksen & Kepert [4]. Linear drag is specified by α^j and the flow is relaxed towards $\tilde{q}^j_{mn}$ with relaxation parameter κ_n.

In (1), the term $D^{jl}_0(m,n)q^j_{mn}$ represents the contribution of the unresolved scales of motion to the overall tendency. The linear operator, $D^{jl}_0(m,n)$, is written in general matrix anisotropic notation, however, in the present calculations it has the isotropic form

$$D^{jl}_0(m,n) = \nu^{jl}_0(n)\ n(n+1) \ , \tag{4}$$

where $n(n+1)$ is the discrete form of the Laplacian operator. Also, the isotropic wavenumber dependent bare viscosity is given by

$$\nu^{jl}_0(n) = \delta^{jl}\ \nu^{jj}_0(T)\ \left(\frac{n}{T}\right)^{\rho^j_0} \ , \tag{5}$$

where δ^{jl} is the Kronecker delta function, which ensures the off-diagonal elements of $\nu_0^{jl}(n)$ are zero. Here, $\nu_0^{jj}(T)$ is the value of the diagonal elements at the truncation wavenumber and the power ρ_0^j controls the steepness of $\nu_0^{jj}(n)$. This means that $\boldsymbol{\nu_0}$, with elements ν_0^{jl}, and hence $\mathbf{D_0}$, with elements D_0^{jl}, are isotropic diagonal matrices.

The time integration of (1), produces the data required to determine the subgrid coefficients necessary for the LES. Details on this procedure are presented in the following section.

3 Stochastic subgrid scale model

The LES has reduced resolution compared with the DNS. The LES wavenumbers are confined to the set

$$\begin{aligned}\mathbf{R} = [\ p,q,r,s \mid -T_R \le p \le T_R\ ,\ |p| \le q \le T_R\ ,\\ -T_R \le r \le T_R\ ,\ |r| \le s \le T_R\ ]\ ,\end{aligned} \tag{6}$$

where T_R is the LES truncation wavenumber and $T_R < T$. The subgrid wavenumber set can then be defined as $\mathbf{S} = \mathbf{T} - \mathbf{R}$. A stochastic subgrid scale model is presented that can replicate the DNS statistics of the large scales whilst truncating the model back from wavenumber set $\mathbf{T}$ to $\mathbf{R}$.

We find that successful LESs result from subgrid scale parameterisations that are inhomogeneous in the vertical and homogeneous but anisotropic in the horizontal. This means that the subgrid scale model can be applied locally in wavenumber space with coupling only in the vertical direction. This is consistent with the Quasi-diagonal Direct Interaction Approximation (QDIA) closure of Frederiksen [2] and the subgrid modelling study of Zidikheri & Frederiksen [7].

To facilitate a discussion on the flow decomposition, for a given wavenumber pair we let $\mathbf{q}$ equal the transpose of (q^1_{mn}, q^2_{mn}). In this vector notation

$$\mathbf{q}_t(t) = \mathbf{q}_t^{\mathbf{R}}(t) + \mathbf{q}_t^{\mathbf{S}}(t)\ , \tag{7}$$

where $\mathbf{q}_t$ is the tendency (or time derivative) of $\mathbf{q}$. Also, $\mathbf{q}_t^{\mathbf{R}}$ is the tendency of the resolved scales where all triad interactions involve wavenumbers less than T_R, and consequently no parameterisation is required. For the remaining subgrid tendency, $\mathbf{q}_t^{\mathbf{S}}$, at least one wavenumber component involved in the triad interactions is greater than T_R. The subgrid tendency can be further decomposed such that

$$\mathbf{q}_t^{\mathbf{S}}(t) = \overline{\mathbf{f}} + \widehat{\mathbf{q}}_t^{\mathbf{S}}(t)\ , \tag{8}$$

where $\overline{\mathbf{f}} \equiv \overline{\mathbf{q}_t^{\mathbf{S}}}$ is the time averaged subgrid tendency, and $\widehat{\mathbf{q}}_t^{\mathbf{S}}$ the fluctuating component. In the present study the values of $\overline{\mathbf{f}}$ are determined from the DNS, and $\widehat{\mathbf{q}}_t^{\mathbf{S}}$ is modelled using the following approach.

The fluctuating component of the subgrid tendency is represented by the stochastic equation

$$\widehat{\mathbf{q}}_t^{\mathbf{S}}(t) = -\mathbf{D_d}\ \widehat{\mathbf{q}}(t) + \widehat{\mathbf{f}}(t)\ , \tag{9}$$

where $\mathbf{D_d}$ is the subgrid drain dissipation matrix, $\widehat{\mathbf{q}}$ is the fluctuating component of $\mathbf{q}$, and $\widehat{\mathbf{f}}$ is a random forcing vector. As the present simulations have two vertical levels, $\mathbf{D_d}$ is a time independent 2×2 matrix, and $\widehat{\mathbf{f}}$ is a time dependent 2 element column vector. $\mathbf{D_d}$ is determined by post-multiplying both sides of (9) by $\widehat{\mathbf{q}}^\dagger(t_0)$, integrating over the decorrelation period τ, and ensemble averaging to remove the contribution of the stochastic backscatter term $\widehat{\mathbf{f}}$. Rearranging for $\mathbf{D_d}$ produces

$$\mathbf{D_d} = -\left\langle \int_{t_0}^{t} \widehat{\mathbf{q}}_t^{\mathbf{S}}(\sigma)\widehat{\mathbf{q}}^\dagger(t_0)d\sigma \right\rangle \left\langle \int_{t_0}^{t} \widehat{\mathbf{q}}(\sigma)\widehat{\mathbf{q}}^\dagger(t_0)d\sigma \right\rangle^{-1}, \tag{10}$$

where $\dagger$ denotes the Hermitian conjugate for vectors and matrices. The angled brackets denote ensemble averaging, with each ensemble member determined by shifting the initial time t_0 and the final time $t = t_0 + \tau$ forward by one timestep. τ is chosen to capture the average subgrid contribution to the resolved scales.

The model for $\widehat{\mathbf{f}}$ is determined by calculating the non-linear noise covariance matrix given by $\mathbf{F} = \boldsymbol{\mathcal{F}} + \boldsymbol{\mathcal{F}}^\dagger$, where $\boldsymbol{\mathcal{F}} = \left\langle \widehat{\mathbf{f}}(t)\ \widehat{\mathbf{q}}^\dagger(t) \right\rangle$. By again post-multiplying both sides of (9) by $\widehat{\mathbf{q}}^\dagger(t_0)$, and adding the conjugate transpose of (9) pre-multipled by $\widehat{\mathbf{q}}(t_0)$ yields the Lyapunov or balance equation

$$\left\langle \widehat{\mathbf{q}}_t^{\mathbf{S}}(t)\widehat{\mathbf{q}}^\dagger(t) \right\rangle + \left\langle \widehat{\mathbf{q}}(t)\widehat{\mathbf{q}}_t^{\mathbf{S}\dagger}(t) \right\rangle = -\mathbf{D_d} \left\langle \widehat{\mathbf{q}}(t)\widehat{\mathbf{q}}^\dagger(t) \right\rangle - \left\langle \widehat{\mathbf{q}}(t)\widehat{\mathbf{q}}^\dagger(t) \right\rangle \mathbf{D_d}^\dagger + \mathbf{F}\ . \tag{11}$$

$\mathbf{F}$ can now be determined given that $\mathbf{D_d}$ has been previously calculated. In general the noise term $\widehat{\mathbf{f}}$ may be coloured, but we find that once $\mathbf{F}$ has been calculated from (11), it is sufficient to model $\widehat{\mathbf{f}}$ as the white noise process $\left\langle \widehat{\mathbf{f}}(t)\ \widehat{\mathbf{f}}^\dagger(t') \right\rangle = \mathbf{F}\ \delta(t-t')$. An eigenvalue decomposition of $\mathbf{F}$ is then used to produce a stochastic model for $\widehat{\mathbf{f}}$.

In the present study, however, we adopt a deterministic expression for the backscatter. We define the backscatter and net linear operators by

$$\mathbf{D_b} = -\boldsymbol{\mathcal{F}} \left\langle \widehat{\mathbf{q}}(t)\ \widehat{\mathbf{q}}^\dagger(t) \right\rangle^{-1}\ , \text{ and} \tag{12}$$

$$\mathbf{D_n} = \mathbf{D_d} + \mathbf{D_b}\ , \tag{13}$$

respectively. The subgrid tendency is then modelled by $\widehat{\mathbf{q}}_t^{\mathbf{S}}(t) = -\mathbf{D_n}\ \widehat{\mathbf{q}}(t)$. The equation solved for the anisotropic LES is

$$\begin{aligned}\frac{\partial q^j_{mn}}{\partial t} &= \mathrm{i}\sum_{pq}\sum_{rs} K^{mpr}_{nqs}\psi^j_{-pq}q^j_{-rs} + \kappa_n(\tilde{q}^j_{mn} - q^j_{mn}) - \mathrm{i}\omega_{mn}\zeta^j_{mn} - \alpha^j\zeta^j_{mn} \\ &- \sum_{l=1}^{2} D^{jl}_0(m,n)q^j_{mn} - \sum_{l=1}^{2} D^{jl}_{\mathrm{n}}(m,n)\widehat{q}^l_{mn} + \bar{f}^j_{mn}\ , \end{aligned} \tag{14}$$

solved over the wavenumber set $\mathbf{R}$. In the anisotropic case each wavenumber pair has a unique $\mathbf{D_n}$. For the isotropic LES, $\mathbf{D_n}$ is averaged over the zonal wavenumbers m, so that it is only a function of the total wavenumbers n. The net eddy viscosity $\boldsymbol{\nu}_\mathbf{n} = \mathbf{D_n}/(n(n+1))$.

4 Scaling of the net eddy viscosity

Various DNS and LES simulations are undertaken to identify how $\boldsymbol{\nu}_\mathbf{n}$ changes with resolution. The highest resolution DNS presented herein has a truncation wavenumber of $T = 504$, and is denoted by T504. This is equivalent to 1536 longitudinal and 768 latitudinal grid points, or a grid point every 0.234 degrees. Along the equator, the distance between grid points is approximately 26km. The time step size for this simulation is $\Delta t = 112$ seconds. All simulations are driven toward $\tilde{q}^j_{mn}$, by the relaxation parameter $\kappa_n = 10^{-6}\mathrm{s}^{-1}$ for $n > 15$ and $\kappa_n = 0$ otherwise. $\tilde{q}^j_{mn}$ consists of a large easterly moving jet in the mid latitudes of each hemisphere, with $\tilde{q}^j_{mn}$ non-zero only for $m = 0$ (i.e. a purely zonal jet). Further details on the structure of $\tilde{q}^j_{mn}$ can be found in Zidikheri & Frederiksen [7]. To be representative of atmospheric flows the layer coupling parameter in SI units is $F_L = 2.5 \times 10^{-12}\mathrm{m}^{-2}$, with $r_{\mathrm{Ros}} = 4.47\times10^5\mathrm{m}$ and a wavelength of $2\pi r_{\mathrm{Ros}} = 2.81\times10^6\mathrm{m}$. The associated non-dimensionalised Rossby wavenumber is $k_{\mathrm{Ros}} = a/r_{\mathrm{Ros}} \approx 14$. It is clear that for all simulations presented within, the large scale Rossby waves are resolved as $k_{\mathrm{Ros}} < T_R < T$.

The anisotropic net eddy viscosity coefficients are calculated from the DNS data using (13) with $\tau = 24\Delta t$. For the T504 data set truncated back to $T_R = 63$, the real component of the anisotropic net eddy viscosity $\nu^{11}_{\mathrm{n}}(m,n)$, is illustrated in Fig. 1. $\nu^{11}_{\mathrm{n}}(m,n)$ generally increase with n and have only a weak dependence on m, and hence are approximately isotropic. $\nu^{22}_{\mathrm{n}}(m,n)$ has similar form to $\nu^{11}_{\mathrm{n}}(m,n)$, but typically 80% of its magnitude. The cross elements $\nu^{12}_{\mathrm{n}}(n)$ and $\nu^{21}_{\mathrm{n}}(n)$ are negligible in comparison. In all cases the mean subgrid tendency $\bar{\mathbf{f}}$ is also found to be negligible. Each of these observations reinforce the use of a diagonal isotropic bare viscosity in

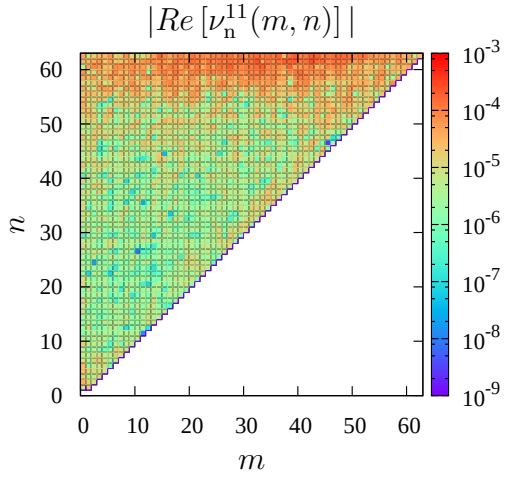

Figure 1: Net eddy viscosity subgrid coefficients $|Re\,[\nu_{\rm n}^{11}(m,n)]\,|$ required to truncate the T504 data set back to an LES data set with $T_R = 63$.

(5). For the remainder of the paper, we will concentrate on the properties of $\nu_{\rm n}^{11}(m,n)$.

The self similarity of the net eddy viscosity coefficients is most clearly illustrated by the isotropised profiles. $\nu_{\rm n}^{11}(m,n)$ is isotropised with $\nu_{\rm n}^{11}(n)$ shown in Fig. 2(a), and exhibits a cusp like shape approaching T_R. The T504 DNS data set is also truncated back to $T_R = 126$ and $T_R = 252$. The resulting profiles of $\nu_{\rm n}^{11}(n)$ are illustrated in Fig. 2(a), along with the bare viscosity profile $\nu_0^{11}(n)$. From this figure it is clear that the maximum value of $\nu_{\rm n}^{11}(n)$ decreases with T_R, with the bare viscosity $\nu_0^{11}(n)$ having the smallest maximum value. This makes sense because as additional scales of motion are resolved by the grid, there are less subgrid scales that must be accounted for by the parameterisation, and the level of eddy viscosity should be reduced. Each of the four profiles are non-dimensionalised by their value at the truncation wavenumber denoted by $\nu_{\rm n}^{11}(T_R)$ (or $\nu_0^{11}(T)$ in the case of the bare viscosity) and plotted in Fig. 2(b) against n/T_R (or n/T for the bare viscosity). This figure accentuates that with this non-dimensionalisation, the steepness of the eddy viscosity profiles increases with the truncation wavenumber.

The change in magnitude and slope of the net eddy viscosity profiles can be quantified by fitting the curves to a power law function. Using a least square approach, the $\nu_{\rm n}^{11}(n)$ profiles are fitted to the function

$$\nu_{\rm n}^{11}(n) = \nu_{\rm n}^{11}(T_R)\ \left(\frac{n}{T_R}\right)^{\rho_{\rm n}^1}\ , \tag{15}$$

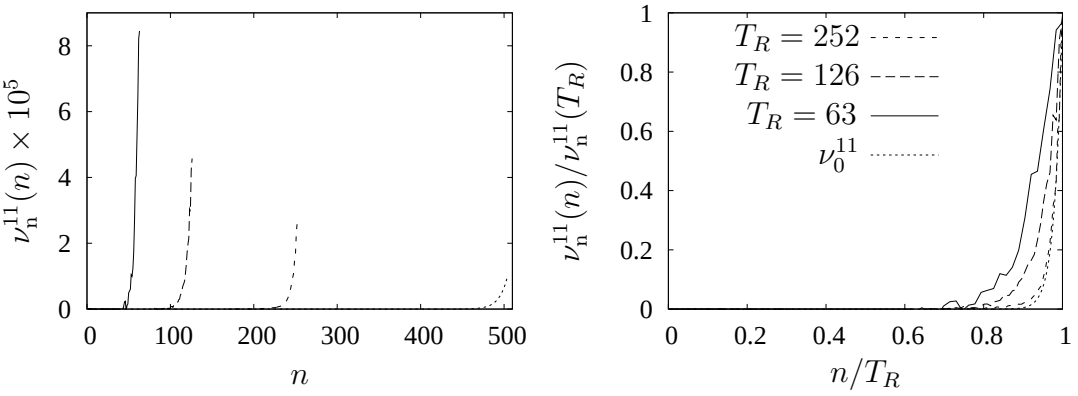

(a) (b)

Figure 2: Isotropic net eddy viscosity subgrid coefficients derived from the T504 DNS data set: (a) $\nu_{\rm n}^{11}(n)$; and (b) non-dimensionalised such that $\nu_{\rm n}^{11}(n)/\nu_{\rm n}^{11}(T_R)$ is plotted against n/T_R. The legend in (b) also represents the data in (a). The bare viscosity ν_0^{11} is also included in these figures.

where $\nu_{\rm n}^{11}(T_R)$ is the value at truncation, and $\rho_{\rm n}^1$ is the exponent. For the T504 DNS truncated back to $T_R = 252$, 126, and 63, the associated values of $\nu_{\rm n}^{11}(T_R)$ and $\rho_{\rm n}^1$ are plotted as upward pointing triangles in Fig 3(a) and Fig 3(b) respectively. $\nu_{\rm n}^{11}(T_R)$ is shown to decrease with T_R, and $\rho_{\rm n}^1$ increases with T_R. This means that as more scales are resolved the net eddy viscosity profiles are reducing in magnitude and becoming steeper, which is consistent with the results in Fig. 2.

Additional DNS calculations are performed to confirm the functional dependence of $\nu_{\rm n}^{11}(T_R)$ and $\rho_{\rm n}^1$ on the LES truncation wavenumber T_R. The new DNS simulations are truncated at $T = 252$ and $T = 126$, with these data sets referred to as T252 and T126 respectively. The $\boldsymbol{\nu_0}$ coefficients of the T252 data set are estimated from $\boldsymbol{\nu_{\rm n}}$ of T504 truncated back to $T_R = 252$. Likewise the $\boldsymbol{\nu_0}$ coefficients of the T126 data set are estimated from $\boldsymbol{\nu_{\rm n}}$ of T504 truncated back to $T_R = 126$. The T252 DNS is in turn truncated back to $T_R = 126$, 63, and 31, with the associated values of $\nu_{\rm n}^{11}(T_R)$, and $\rho_{\rm n}^1$ plotted as downward pointing triangles in Fig. 4. The T126 DNS is truncated back to several levels between $T_R = 31$ and 63, with the values of $\nu_{\rm n}^{11}(T_R)$, and $\rho_{\rm n}^1$ plotted as open circles. A least squares trend line is fit to the $\nu_{\rm n}^{11}(T_R)$ data points in Fig 3(a) producing the functional dependence

$$\nu_{\rm n}^{11}(T_R) = 0.006/T_R \ , \tag{16}$$

with a correlation coefficient of 0.997. A least squares trend line is also fit to

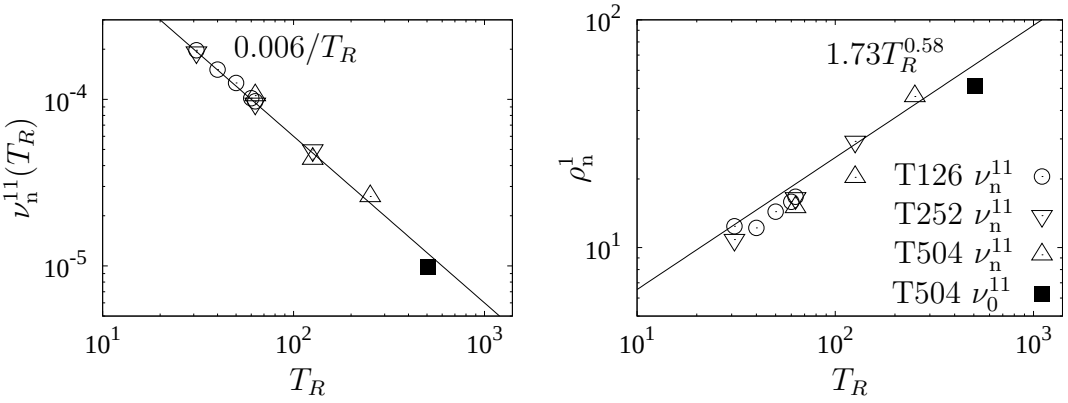

(a) (b)

Figure 3: The scaling of the subgrid coefficients properties: (a) $\nu_{\rm n}^{11}(T_R)$; and (b) $\rho_{\rm n}^1$, determined from three DNS data sets T504, T252 and T126 truncated back to various values of T_R. The legend in (b) also represents the data in (a).

the $\rho_{\rm n}^1$ data points in Fig 3(b) producing the function

$$\rho_{\rm n}^1(T_R) = 1.73 T_R^{0.58} \ , \tag{17}$$

with a correlation coefficient of 0.960. The values of ν_0^{11} and ρ_0^{11} for the T504 DNS are also plotted on Fig 3(a) and Fig 3(b) respectively as solid squares, and follow the trend line. The degree to which the scaling laws governing $\boldsymbol{\nu_{\rm n}}$, are consistent with the prescribed $\boldsymbol{\nu_0}$, are addressed in the following section.

5 Self consistency of the bare viscosity

Just as the bare viscosity $\boldsymbol{\nu_0}$ represents the contribution of the unresolved scales in the DNS to the tendency over the wavenumber set $\mathbf{T}$, the net eddy viscosity $\boldsymbol{\nu_{\rm n}}$ represents the contribution of the subgrid scales $\mathbf{S}$ to the tendency of the LES resolved scales $\mathbf{R}$. It is, therefore, proposed that the scaling observed for $\boldsymbol{\nu_{\rm n}}$, is also applicable to $\boldsymbol{\nu_0}$. It was shown previously in Fig. 3 that $\boldsymbol{\nu_{\rm n}}$ and $\boldsymbol{\nu_0}$ have consistent scaling. The sensitivity of this result is assessed below. As an additional check, DNS simulations are run with $\boldsymbol{\nu_0}$ profiles generated using the scaling functions. The resulting spectra are compared to the spectra from the highest resolution T504 case.

Thus far the scaling laws for $\boldsymbol{\nu_{\rm n}}$ have been identified by running a series of DNS simulations with a prescribed $\boldsymbol{\nu_0}$ truncated at various T_R. The sensitiv-

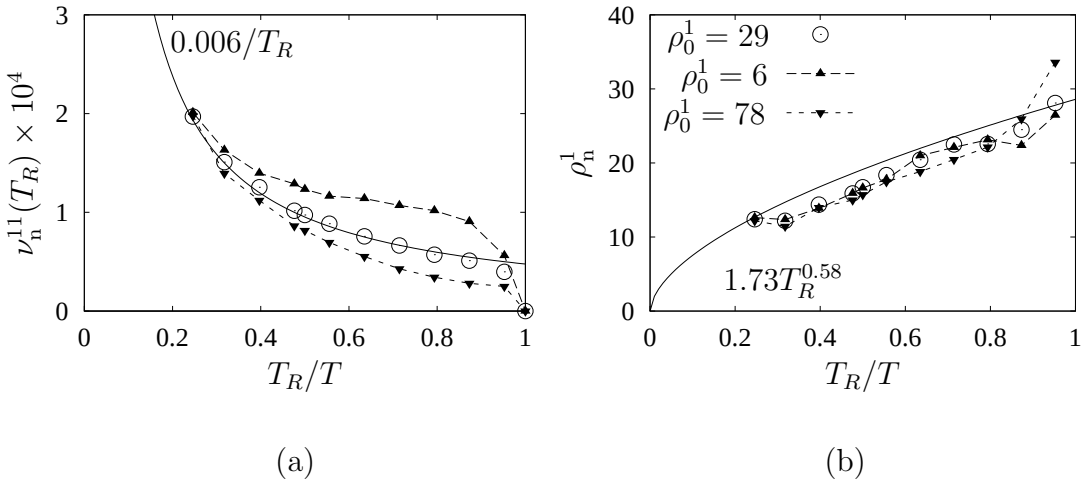

(a) (b)

Figure 4: Using the T126 DNS data set, the sensitivity to ρ_0^1 of the subgrid coefficients properties: (a) $\nu_{\rm n}^{11}(T_R)$; and (b) $\rho_{\rm n}^1$, for various values of T_R. The legend in (b) also represents the data in (a).

ity of the results is now determined by running additional DNS simulations with varying $\boldsymbol{\nu_0}$. Specifically the T126 DNS is run with three different bare viscosity profiles, each of which are truncated back to several levels between $T_R = 31$ and 126. In each case $\boldsymbol{\nu_0}$ is calculated according to (5), with $\nu_0^{jj}(T_R)$ fixed and equal to $\nu_{\rm n}^{jj}(T_R)$ of the T504 DNS truncated back to $T_R = 126$. Three different values of ρ_0^j are used: $\rho_0^j = 29$, consistent with the previous T126 DNS; $\rho_0^j = 6$, a typical value used in atmospheric DNS studies; and $\rho_0^j = 78$, chosen to illustrate the impact of an excessively large value. The impact of the $\boldsymbol{\nu_0}$ profiles on $\nu_{\rm n}^{11}(T_R)$ at various T_R is first assessed. The trend line from Fig. 3(a) is included in Fig. 4(a), but this time plotted on a linear scale with T_R/T the independent variable. The DNS calculations are repeated with $\rho_0^j = 29$, 6 and 78, and the resulting values of $\nu_{\rm n}^{11}(T_R)$ added to Fig. 4(a). The values of $\nu_{\rm n}^{11}(T_R)$ appear to deviate from each other for $T_R/T > 0.5$. The same is true regarding the agreement of $\rho_{\rm n}^1$ determined from the various DNS simulations in Fig. 4(b). In general, the closer T_R is to T the greater influence $\boldsymbol{\nu_0}$ has on $\boldsymbol{\nu_{\rm n}}$. In close proximity to T, however, $\nu_{\rm n}^{11}(T_R)$ approaches zero regardless of $\boldsymbol{\nu_0}$. This is because there are no subgrid scales at $T_R = T$, and by definition $\boldsymbol{\nu_{\rm n}} = 0$. To ensure the limiting case at $T = T_R$ and the prescribed $\boldsymbol{\nu_0}$ had minimal impact on the scaling functions describing $\boldsymbol{\nu_{\rm n}}$, the trend lines in Fig. 2 were only fit to data points with $T_R/T \leq 0.5$.

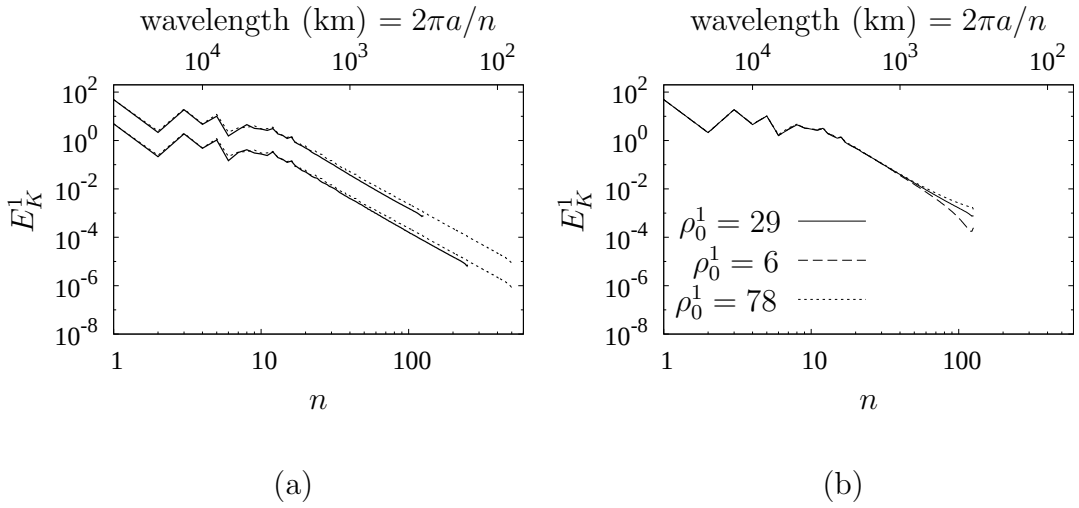

Figure 5: Comparison of the kinetic energy spectra on level 1 (E_K^1) between: (a) the T504 DNS and the T126 DNS (top spectra), and with the T252 DNS (bottom spectra, shifted down one decade for clarity); and (b) the T126 DNS using three different power laws with $\rho_0^j = 29$, 6, and 78.

We now verify that a lower resolution DNS with $\boldsymbol{\nu_0}$ defined using the scaling laws can replicate the statistics of a higher resolution DNS. A comparison is made between the time and m averaged kinetic energy spectra on level 1 (E_K^1) resulting from the T504, T252 and T126 DNS simulations. The $\boldsymbol{\nu_0}$ profiles for the T252 and T126 DNS are determined using the scaling functions (16) and (17) in conjunction with (5). Figure 5(a) illustrates good agreement between the E_K^1 from each of the DNS simulations. Importantly the energy in the low wavenumber large scales of motion agree. In the higher wavenumbers, the lower resolution cases decay slightly faster than the T504 case. The implications of using the incorrect scaling for $\boldsymbol{\nu_0}$ is illustrated with application to the T126 DNS. Figure 5(b) illustrates E_K^1 resulting from the T126 DNS simulations with $\rho_0^j = 29$, 6 and 78. The spectra labelled $\rho_0^j = 29$ is the same as the T126 DNS spectra in Fig 5(a). The spectra labelled $\rho_0^j = 78$ produces a turn up at the end of the spectra due to the net eddy viscosity dropping off more rapidly. The spectra from the $\rho_0^j = 6$ case rapidly decays at the higher wavenumbers, with a turn up at the tail of the spectra. If the incorrect $\boldsymbol{\nu_0}$ is applied, the tails of the energy spectra are not correctly represented, however, at these resolutions the large scales still seem to be adequately captured.

6 Concluding remarks

Data from a two level quasigeostrophic atmospheric model has been generated using DNS. Subgrid parameterisations comprising of a net eddy viscosity were generated from the DNS data at various truncation levels. A self similar scaling law for the net eddy viscosity was determined from the results. The scaling laws may remove the need to produce high resolution reference DNS data sets, which would widen the applicability of LES method to more general cases.

Acknowledgements: V. Kitsios would like to acknowledge the CSIRO Office of the Chief Executive for funding his post-doctoral position.

References

[1] J. S. Frederiksen. Precursors to blocking anomalies: the tangent linear and inverse problems. *J. Atmos. Sci.*, 55:2419–2436, 1998.

[2] J. S. Frederiksen. Subgrid-scale parameterizations of eddy-topographic force, eddy viscosity and stoachstic backscatter for flow over topography. *J. Atmos. Sci*, 56:1481–1493, 1999.

[3] J. S. Frederiksen and A. G. Davies. Eddy viscosity and stochastic backscatter parameterizations on the sphere for atmospheric circulation models. *J. Atmos. Sci*, 54:2475–2492, 1997.

[4] J. S. Frederiksen and S. M. Kepert. Dynamical subgrid-scale parameterizations from Direct Numerical Simulations. *J. Atmos. Sci.*, 63:3006–3019, 2006.

[5] C. E. Leith. stochastic backscatter in a subgrid-scale model: Plane shear mixing layer. *Phys. Fluids*, 2(3):297–299, 1990.

[6] J. Smagorinsky. General circulation experiments with the primitive equations: I. the basic experiment. *Monthly Weather Review*, 91(3):99–164, 1963.

[7] M. J. Zidikheri and J. S. Frederiksen. Stochastic subgrid parameterizations for simulations of atmospheric baroclinic flows. *J. Atmos. Sci.*, 66:2844–2858, 2009.